The International Journal of Advanced Manufacturing Technology (2023) 129:2823–2841
https://doi.org/10.1007/s00170-023-12469-9

ORIGINAL ARTICLE

Exploring wide-parametric range for tool electrode selection based on surface characterization and machining rate employing powder-mixed electric discharge machining process for Ti6Al4V ELI

Muhammad Umar Farooq[1] · Saqib Anwar[2] · Muhammad Asad Ali[3] · Abual Hassan[4] · Ray Tahir Mushtaq[5]

Received: 25 June 2023 / Accepted: 3 October 2023 / Published online: 19 October 2023

Abstract
The titanium alloy Ti6Al4V ELI (grade 23) is widely used in biomedical industry because of its engineering attributes. However, it requires surface modifications and has processing challenges because it is difficult to machine nature. Therefore, powder-mixed electric discharge machining process is commonly applied to simultaneously machine the material and carry out surface treatment. The performance of the process is limited by both low cutting efficiency and the formation of a rough surface. In this regard, the current study evaluates SiC powder-mixed electric discharge machining of Ti6Al4V ELI using a range of tool materials such as copper, brass, graphite, and aluminum along with a comprehensive list of process parameters. The surface roughness parameters involving arithmetic roughness, the average peak-to-valley distance, and the highest peak-to-deepest valley distance along with material removal rate are comprehensively studied. Taguchi design of experiments L_{16} orthogonal array is used to study the process performance with parametric effect analysis, parametric significance analysis, and surface morphological analysis with a scanning electron microscope. Furthermore, the experimental results are optimized against a multi-response optimization matrix using grey relational analysis approach. An optimal compromise between surface attributes and cutting efficiency is identified by Al electrode, pulse current of 14 A, pulse on time of 75 µs, pulse off time of 75 µs, and negative polarity parametric conditions.

Keywords Titanium Alloy · Ti6Al4V · Electrical discharge machining · Surface topography · Grey relational analysis

1 Introduction

The aeronautical and automotive industries use titanium and its alloys in various advanced applications such as airframes, landing gear, fastening elements, engine components, and axle shafts. The considerable properties which make these materials preferable include strength-to-weight ratio, toughness, corrosion and fatigue resistance, and high-performance ability at extreme temperatures. Among different variants of titanium, Ti6Al4V is widely used because of its durability and engineering attributes required for specialized applications. However, there are certain limitations of the material which makes its machinability challenging such as low thermal conductivity and reactivity [1]. These limitations drive manufacturing industries to choose non-conventional processing methods for machining and surface modification purposes. In addition to this, the use of conventional processes is also limited because of the uneconomical machinability of hard-to-cut alloys and composites resulting from tooling costs (owing to physical tool/workpiece

✉ Muhammad Umar Farooq
mn21muf@leeds.ac.uk; Umarmuf0@gmail.com

[1] School of Mechanical Engineering, University of Leeds, Leeds LS2 9JT, UK

[2] Industrial Engineering Department, College of Engineering, King Saud University, P.O. Box 800, 11421 Riyadh, Saudi Arabia

[3] Department of Industrial and Manufacturing Engineering, University of Engineering and Technology, Lahore, Pakistan

[4] Faculty of Mechanical Engineering and Ship Technology, Gdansk University of Technology, Gdansk, Poland

[5] Bio-Additive Manufacturing University-Enterprise Joint Research Center of Shaanxi Province, Department of Industry Engineering, School of Mechanical Engineering, Northwestern Polytechnical University, Xi'an 710072, People's Republic of China

contact-induced wear, residual stresses, and mechanical failure) [2, 3]. Therefore, electric discharge machining, laser beam and electron beam machining, water jet, and other processes are employed for efficient machining and surface modification. The electric discharge machining (EDM) is one of the cutting-edge processes used in manufacturing industries to simultaneously machine and modify work surface for advanced applications. Moreover, the process is efficient to fabricate intricate geometries with high precision and improve the mechanical properties of surface [4]. The electric discharge machining is a stochastic thermo-electric process which erodes the conductive materials through spark-induced thermal energy. The tool (having an inverse shape of desired geometry on workpiece) and workpiece are brought significantly close leading to sparking activity while having dielectric medium in the inter-electrode gap. Both electrodes act as a capacity with no physical contact; therefore, no mechanical-induced residual stresses are expected in the workpiece [5].

To further enhance the functionalities of the process, different researchers have developed technologies which aid in thermo-electric conditions. The dielectric medium is modified using biodegradable oils, emulsions, surfactants, and conductive or non-conductive particles. Similarly, the tool electrodes are improved through manufacturing techniques such as powder metallurgy or with thermal treatments for instance quenching or cryogenics. Since the process is highly dependent on electric science, therefore, different parametric approaches are used to optimize desired objectives by altering sparking conditions. A thorough review of works presented in this domain is presented in Table 1.

The researchers have modified process and investigated different objectives under the electric discharge machining process. For instance, Guu et al. [13] evaluated the machinability of AISI D2 steel and found that pulse current-induced discharge energy significantly affected the erosion rate and surface finish. Gattu and Yan [14] machined tungsten carbide using powder-mixed dielectrics. The authors used insulative, conductive, and semiconductive powders such as alumina powder (Al_2O_3), carbon nanofiber (CnF), and silicon (Si), respectively. The authors found that addition of powder improved inter-electrode energy transfer and resulted in a higher material removal rate and less roughness. The Al_2O_3 showed small-sized craters on the surface. Pradhan et al. [15] reported the effect of pulse on time for the machining of titanium superalloy. Pradhan et al. found that at higher pulse on time, material removal spikes up from 0.0062 to 0.033 mg/min owing to prolonged exposure time to discharge energy. Ekmekci and Efe [16] evaluate the performance of nano- and micro-additives on the machined surfaces of Ti6Al4V using pure Ti (grade 2) as electrode. The authors showed that the micro-hydroxyapatite-mixed dielectric with pulse current 7 A and pulse on time 400 µs resulted in the lowest roughness of 2 µm, whereas the nano-hydroxyapatite-mixed dielectric with pulse current 22 A and pulse on time 1600 µs produced 9 µm roughness. The authors found that the pressure drop at the end of the sparking directs the dielectric to remove the melt pool on the surface. In this aspect, the addition of powder in the dielectric improved discharge activity by dividing the major plasma channel to different branches. Surya and Gugulothu [17] carried out machining of 7075–4% TiC aluminum composite using graphite powder. The authors discussed the formation of small cavities on the surface as a result of broken discharges because of powder particles in dielectric. The material removal rate is directly affected by discharge energy and the increase in pulse on time deteriorated the surface. Kumar et al. [18] evaluated the machinability of carbon fiber-reinforced polymers under the influence of SiC powder. The authors found that 4 g/L SiC powder concentration, 1 A pulse current, and 15 µs resulted in the least surface roughness of 1.2 µm. Rehman et al. [19] machined EN-30B alloy steel using copper tool and graphite powder mixed in dielectric. The authors found that 4 g/L particle concentration of 20 µm with 12 A pulse current and 45 µs pulse on time resulted in the highest material removal rate. Darji et al. [20] evaluated the performance of chromium powder-mixed electric discharge machining of Inconel 718. The authors showed 5 g/L powder concentration reduced surface defects and resulted in the lowest roughness of 4.73 µm. Similarly, Vora et al. [21] carried out the machining of Nitinol alloy using nano-graphene-mixed electric discharge machining process. The authors quantified the influence of powder concentration (0–2 g/L), pulse current (5–15 A), pulse on time (3–9 µs), and pulse off time (2–8 µs). The authors achieved 2.92 µm roughness using 8 µs pulse on time, 6 µs pulse off time, 2 g/L powder concentration, and 6 A pulse current.

Along with advancements in dielectrics, different researchers have employed parametric optimization approaches to achieve the desired compromise. Majumdar et al. [22] optimized the nano-graphene-mixed electric discharge machining process for Inconel 625. The authors used powder concentration, pulse current, and pulse on time as input variables for the assessment of material removal rate using Taguchi design of experiments. The signal/noise ratio-based optimization resulted 0.4 g/L, 12 A, and 50 µs against ~ 7.65% error as optimized results. Thakur et al. [23] used response surface methodology and artificial neural networks to optimize the machining of Al LM-25/SiC composite. The authors found that machine parameters directly influencing energy deposition significantly affect surface integrity, whereas Kumar et al. [24] improved the surface quality of Inconel 706 by introducing magnetic field in the process. The authors used grey relational analysis to optimize the process for surface roughness, material removal rate, and tool wear rate. The grey relational analysis showed

Table 1 State-of-the-arts presented to improve processability attributes

Authors, year, and reference	Tool electrode, workpiece, and experimental conditions	Response characteristics and optimization approach	Findings
Mughal et al. 2021 [6]	Copper; Ti6Al4V ELI; SiC powder concentration, pulse current, pulse on/off time	Surface roughness (Ra), recast layer thickness; desirability function	The SiC-mixed EDM resulted in improved surface quality as compared to conventional kerosene-based EDM
Ahmed et al. 2019 [7]	Aluminum, copper, brass, graphite; Ti6Al4V; pulse current, pulse ratio, polarity	Surface roughness (Ra), tool wear rate, overcut, material removal rate; graphical-compromise	The graphite electrode produced Ra = 8.85 µm rougher surface as compared to others. None of the electrode could produce micro-impressions without compromise
Li et al. 2017 [4]	Copper; Ti6Al4V; SiC powder concentration, pulse current	Surface morphology, microhardness; none	The crater boundaries were found clearer in the case of SiC-mixed EDM as compared to conventional EDM
Al-Amin et al. 2021 [8]	Ti6Al4V; 316L; pulse current, HA powder concentration, pulse on time, duty cycle	Material removal rate, surface roughness (Ra), tool wear rate; S/N ratio, multi-objective spotted hyena optimizer	A compromise between discharge energy was developed to produce low roughness and tool wear and a high erosion rate with errors of less than 10%
Goyal et al. 2022 [9]	Zinc-coated brass; AZ31 alloy; pulse on and off time, servo voltage	Surface roughness (Ra, Rz), microhardness, material removal rate; grey wolf optimization (GWO) algorithm	The surface defects were observed on the surface, which originate from thermos-electric physics. The compromise between responses was found with a 6.3% error
Baroi et al. 2023 [10]	Brass; Ti6Al4V ELI; boric acid powder concentration, pulse current, pulse on and off time	surface roughness (Ra), specific energy consumption, material removal rate, tool wear rate; Overall evaluation criteria ranking	The powder-mixed dielectric has improved surface roughness which is significantly affected by discharge energy from pulse current and pulse on time
Isik et al. 2023 [11]	Copper; WC-15Co; pulse current, pulse on and off time	Surface roughness (Ra), material removal rate, tool wear rate; Taguchi-grey relational analysis	The pulse current 44.23%, pulse on time 28.77%, and pulse off time 5.87% controlled process grey relational grade
Bhowmick et al. 2023 [12]	Copper; Inconel 718; titanium powder concentration, pulse current, gap voltage, pulse on and off time	Surface roughness (Ra), material removal rate; response surface methodology-fuzzy logic	The process was optimized with error under 10%. The increase in pulse current and pulse on time resulted significant rise in roughness

Table 2 Chemical composition of workpiece material

Elements	Al	C	H	Fe	N	O	V	Ti
Wt. (%)	5.89	0.016	0.0019	0.14	0.007	0.1	3.96	Balance

that pulse on time 62.84%, pulse current 28.64%, and pulse off time 8.50% controlled overall response characteristics. The optimized parametric conditions pulse current 5 A, pulse on time 50 µs, and pulse off time 20 µs resulted least roughness 1.66 µm. Chakraborty et al. [25] used response surface methodology, grey relational analysis, and particle swarm algorithm to optimize the machining of Ti6Al4V using Al_2O_3 powder. The surface roughness of 1.38 µm was achieved using 4 g/L powder concentration and 2 A pulse current. Ishfaq et al. [26] carried out the machining of AISI D2 steel using copper electrode. The authors used desirability function to optimize the process for dimensional errors.

The literature survey has highlighted that Ti6Al4V, a hard-to-machine material, is processed through electric discharge machining employing different technologies. Based on the use cases, the machining objectives and their associated challenges are investigated based on parametric conditions and modified dielectrics. The literature identifies SiC powder-mixed electric discharge machining process has significantly improved surface characteristics and machinability. However, all surface roughness parameters and their parametric correlation are not comprehensively evaluated which is done herein. In addition, a range of process variables are evaluated against four types of electrode materials to determine the best processing conditions depending on surface morphology, roughness, and cutting efficiency. Moreover, the grey relational analysis-based multi-objective optimization approach is used to optimize the response variables such as arithmetic mean, average peak-to-valley distances, and material removal rate. As the responses are conflicting in nature, therefore, the robustness of the optimized dataset was ensured through confirmatory experimentation. The physics of electric discharge machining process is correlated with the experimental results and scanning electron microscopic evidences.

2 Materials and methods

The Ti6Al4V ELI as workpiece is used to carry out experiments. The material was procured from BaoJi Titanium Industry Co. Ltd., China, and the composition is verified with the manufacturer sheet as provided in Table 2.

The alloy is specially used in high-performance applications because of its physical properties. Different machine elements in aeronautical industries and different implants in biomedical industries are the major application areas. The potential physical properties that make the alloy preferable in the abovementioned applications and influence the processing conditions in electric discharge machining are tabulated in Table 3.

Table 3 Physical properties of workpiece material

Properties	Units	Value
Density	g/cm^3	4.43
Yield strength	MPa	955
Ultimate tensile strength	MPa	990
Thermal conductivity	$W\text{-}m^{-1}\ K^{-1}$	6.7
Electrical resistivity	µΩ-cm	178
Melting point	°C	1660

Table 4 Thermo-physical properties of tool electrodes (open access [7])

Tool material	Thermo-physical properties			
	Density ($g\text{-}cm^{-3}$)	Melting point (°C)	Thermal conductivity ($W\text{-}m^{-1}\ K^{-1}$)	Electrical conductivity ($S\text{-}m^{-1}$)
Graphite	1.77	3300	400	0.3×10^6
Copper	8.90	1083	385	59.6×10^6
Brass	8.73	940	109	16×10^6
Aluminum	2.75	660	205	35×10^6

The objective of the work is to evaluate the surface roughness parameters along with process efficiency. Therefore, a range of potential electrode materials are selected based on their electrical and thermal properties. The machining process involves thermo-electric multiphysics dynamics; therefore, the selection of tool materials is not straightforward for Ti6Al4V ELI. The potential uncertainty is derived from electrical and thermal conductivities of materials which control melt dynamics and vaporization of work surface. The tool electrodes, having 15 mm diameter, copper (Cu), aluminum (Al), graphite (Gr), and brass (Br), are used. The physical properties which are important during processing are given in Table 4.

The CNC Electric Discharge Machine Die-Sinking (RJ—230 creators: Taiwan) was used to machine 300-µm circular cavities. The research methodology is shown in Fig. 1. As per guidelines from the literature on achieving high surface integrity, SiC-mixed dielectric was employed because of its superior electrical resistivity and thermal conductivity [4, 18]. The physical properties which facilitate plasma formation and machinability are mentioned in Table 5. The

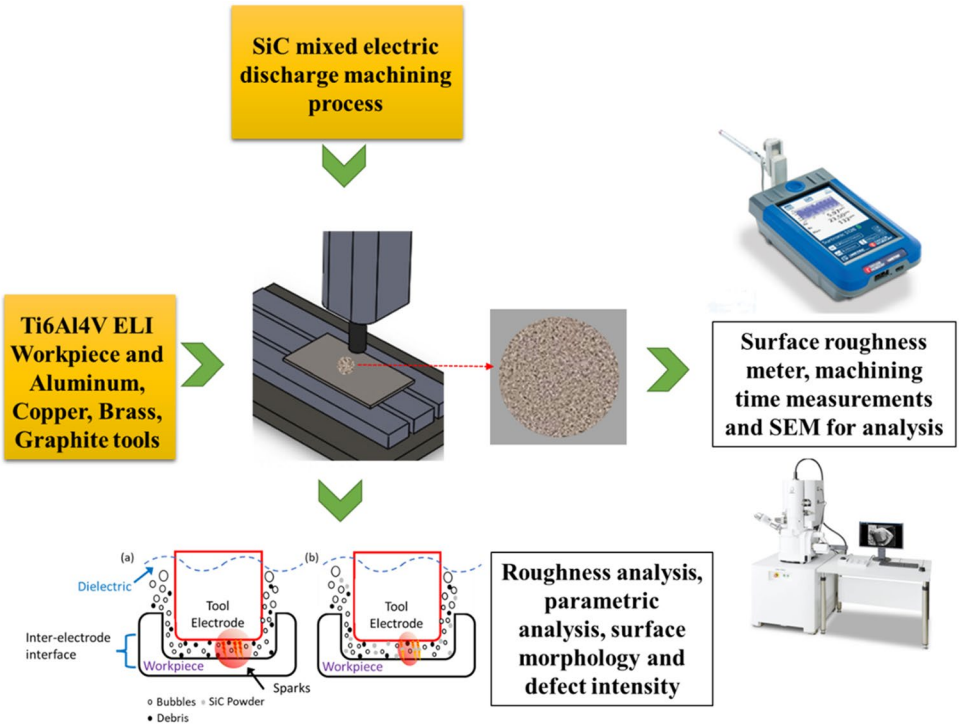

Fig. 1 Experimental methodology

Table 5 Physical properties of SiC powder and dielectric [4, 27]

Property	SiC	Kerosene	Unit
Nominal diameter	70–80	-	µm
Density	3.2	0.81	g/cm^3
Specific heat	510–560	2100	J/Kg K
Thermal conductivity	300	0.14	W/m K
Electrical resistivity	0.01–1	-	µΩ-cm

Table 6 Experimental details [28]

Parameters	Levels
Electrode type	Aluminum (Al), copper (Cu), brass (Br), graphite (Gr)
Electrode diameter	15 mm
Workpiece	Ti6Al4V ELI
Workpiece dimensions	100 × 100 × 4 mm^3
Pulse current	8, 10, 12, 14 A
Pulse on time	50, 75,100, 125 µs
Pulse off time	25, 50, 75, 100 µs
Polarity	+, −
Dielectric	Kerosene oil + 5 g/L SiC
Cavity depth	300 µm

SiC powder has higher thermal conductivity and density as compared to kerosene oil. Therefore, 5 g/L concentration was mixed during the experiments to improve tool-electrode interfacial sparking.

Firstly, a two-phase experimental campaign was used including preliminary experimentation which involved parameter selection and suitability determination of the levels. Secondly, the Taguchi design of experiments-based approach was used for parametric assessment and response characterization. In the preliminary experimentation, the criteria of parametric selection included substantial difference in surface attributes/material removal rate, complete impression of cut, low burn marks, and effective sparking. The parametric levels which resulted in insufficient sparking, incomplete machining cycle, and poor surface quality were not chosen for the design of experiments. The experimental details are shown in Table 6 representing detailed characteristics, parametric levels, and machining details. The surface roughness Ra was thoroughly analyzed in the previous project [28], which is also taken into account to consider complete process effects. Taguchi orthogonal array L_{16} is used with four levels of electrode type, pulse on time, pulse off time, and pulse current using Minitab software v2022.

A uniform procedure was ensured during experiments to rule out external variabilities caused by unbalanced positioning and clamping. Each experiment was carried out with a new tool for surface morphological studies and to avoid any heat treatments of tool itself. The surface roughness attributes such as arithmetic mean Ra, highest peak and the deepest valley distance Rt, and average peak-to-valley distance Rz were measured using Taylor

Hobson surface texture meter (UK) with cutoff length 0.8 mm and evaluation length 4 mm. Five different points on the surface were selected for roughness measurement and the average was used for parametric analysis. To characterize surface and study morphology, Quanta 450 field emission gun scanning electron microscopy was used. The surface morphology obtained by each electrode is analyzed and compared qualitatively with correlations to quantitative trends. Similarly, a precision weight balance was used to measure the weight of workpiece before and after machining with 0.001 g of least count. The difference in weight is processed with machining time required to machine 300-µm cavity to result in material removal rate. All response parameters such as arithmetic mean Ra, highest peak and the deepest valley distance Rt, average peak-to-valley distance Rz, and material removal rate are further processed through analysis of variance to determine parametric significance and grey relational analysis for optimized results.

3 Results and discussion

Thorough preliminary and mature experimentation phases were completed to analyze the machinability and evolved surface of Ti6Al4V through different electrode materials under various conditions. In addition, comprehensive statistical as well as morphological analyses were carried out to improve cutting efficiency and surface integrity.

3.1 Parametric control analysis

Parametric control analysis is performed to evaluate the influence over response parameters. The main effect plots are generated, which describe the behavioral patterns of response measures with increasing values of machining factors to characterize the physics involved in the process [29]. The parametric trends of all the significant control variables are discussed in relation to physical science.

3.1.1 Roughness—arithmetic mean Ra

The machining is carried out using a constant SiC powder concentration of 5 g/L in dielectric to obtain improved dielectric properties. The powder particles reduce the electrical resistivity of dielectric medium by distributing the plasma channel to multiple routes. The impulse forces are reduced in the discharge gap because of powder particles breaking the spark channel. The mechanism results in a balanced distribution of spark energy creating melting on the surface. Employing the mechanistic benefits of powder-mixed dielectric, different tool electrodes are employed based on their thermal conductivities which aid in material removal mechanism. The graphite electrode produced a relatively higher mean roughness Ra, and the aluminum electrode resulted in relatively least Ra, as shown in Fig. 2. Gr produced the highest surface roughness of 14.16 µm. Referring to Fig. 2, it is observed that Al having the lowest melting temperature of 660 °C, in all selected tool materials, resulted the lowest surface roughness around 5.1 µm with less temperature effect (as evident in the micrographs in Fig. 2). However,

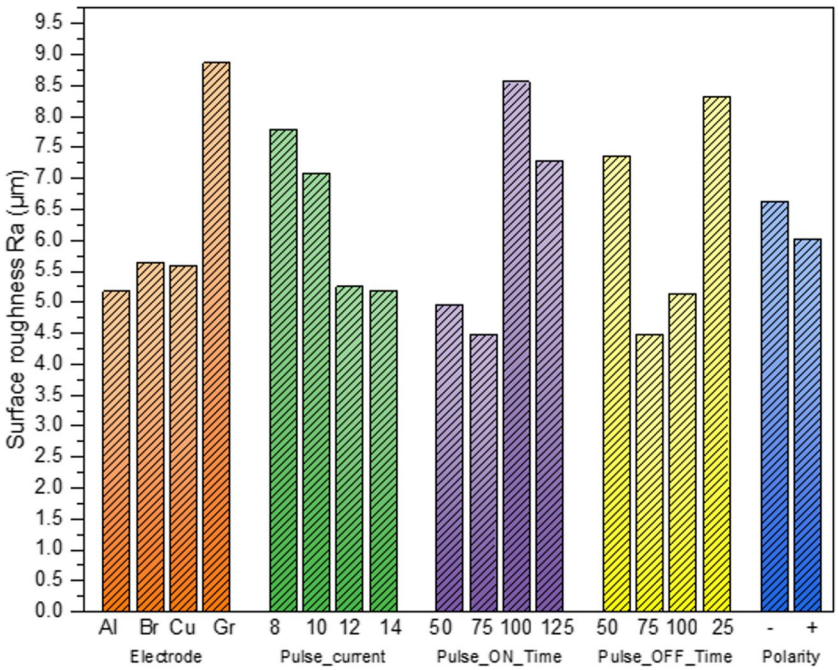

Fig. 2 Main effect plot for the arithmetic mean (Ra)

brass, copper, and graphite with higher melting temperatures 940 °C, 1089 °C, and 3300 °C, respectively, melted and vaporized more material and produced a surface with large and deep craters. A higher surface roughness value recorded for graphite was around 9.1 µm. Ahmed et al. [30] evaluated the role of material on surface roughness, showing that graphite is the electrode with the highest thermal energy, and the high melting point helps to erode the more workpiece material with larger cavities, resulting in rougher surfaces compared to brass and copper electrode.

Figure 2 shows the impact of pulse current on Ti6Al4V surface roughness Ra values. Initially, at 8 A pulse current, material from the surface eroded with deeper craters giving rise to Ra to ~ 7.5 µm. However, the dissipation of the heat was not balanced because of the poor thermal conductivity of Ti6Al4V. Therefore, with the increase in pulse current, the discharge energy density was increased, reflecting the increased volume of the melt pool. The effect breaks the dielectric and generates carbon constituents. These carbon constituents settle down on the workpiece surface and hinder material erosion, with small and shallow craters forming on the surface. Therefore, increasing the pulse current up to 14 A reduced the surface roughness Ra value by around 5 µm. A similar effect was experienced in literature where a balanced correlation of higher current values with improved flushing control was recommended [31]. Conclusively, a higher pulse current produces an improved surface and helps remove unwanted material efficiently.

The effect of pulse on time on the Ra is illustrated in Fig. 3, which is directly related to increased material removal and higher surface roughness. At 50 µs, a low roughness of 5 µm was recorded. Further increase in pulse on time at 100 µs erodes more material with deeper craters, and Ra rose to ~ 8.7 µm. At 75 µs and 125 µs decreasing trend in Ra, values were observed due to debris accumulation between the inter-electrode gaps. In addition, improper flushing causes dispersal of the spark, resulting in low material erosion and smaller craters on the surface with decreased Ra values. When the spark generation is increased, the discharge energy gets denser, and the impulsive force of the spark erodes the work part resulting in larger and deeper interconnected craters. The higher difference of surface profile from the mean line reflects in increased roughness Ra. Al Amin et al. [8] studied that the increase in pulse current and pulse on time enhances the density of plasma channel that will ionize the more material and surface roughness increased of 316L steel.

An increase in pulse off time promotes the proper flushing time and cooling of melted material over the machined surface. At the low pulse off time 25 µs, low flushing action is performed to remove debris which results in compromised, unwanted material removal and produces high 8.5 µm roughness (Fig. 2). The increase in off time balances of spark generation time and flushing action, which reduce Ra to ~ 4.2 µm showing relatively 50.58% decrease. Furthermore, an increase beyond a certain threshold destabilized melt pool dynamics which resulted in ~ 11.90% increase (4.7 µm at 100 µs). A similar physics was observed in the literature [32]. In the negative polarity, high discharge energy is distributed at the positive electrode, which results in uniformly distributed deeper cavities with a higher roughness Ra of 6.6 µm. In the positive polarity, more charge is distributed on the tool electrode, and less workpiece erosion is observed. This reduced roughness by ~ 12%, a similar behavior reported in another study [33]. Samples machined with different conditions are shown in Fig. 3. Dong et al. [31] concluded that polarity helps to generate a strong and dense plasma channel which forms large cavities with increased material removal.

The surface morphology of Ti6Al4V produced through aluminum electrode is shown in Fig. 4. The evidence of patches of smooth surface, craters, and redeposits is highlighted. The aluminum electrode has the lowest melting temperature among others. The heat transfer in the tool-workpiece interaction zone melts the tool material (melting temperature 660 °C) significantly as compared to workpiece material which has a higher melting temperature of 1660 °C. The melt material is redeposited on the surface during pulse off time and creates a brittle recast layer. The cracks are also formed on the surface because of the brittleness of titanium oxides and carbides. Isik et al. [11] discussed a similar mechanism which forms irregularities on the surface during machining of cemented carbide. The authors showed microcracks, surface damage, and crater formation on the recast layer because of thermal energy transfer. Conclusively, the synergistic effect of high discharge current (effectively channeled through powder particles) and flushing time results in sufficient heat formation in the interaction zone showing high melting and vaporization activity. The flushing action removes melt material which forms low degree of damage. Similarly, the powder particles distribute the discharge energy in a balanced manner preventing the formation of deep craters and other defects. These mechanisms combined result in low arithmetic roughness. A similar mechanistic phenomenon is endorsed by Ahmed et al. [7] and Darji et al. [20].

3.1.2 Roughness—highest peak and the deepest valley distance Rt

A similar trend is observed (Fig. 5) for Rt, which is the highest peak and the deepest valley distance. It influences tribological applications as the peaks with smoothened forming debris which sometimes are considered hazardous to the environment.

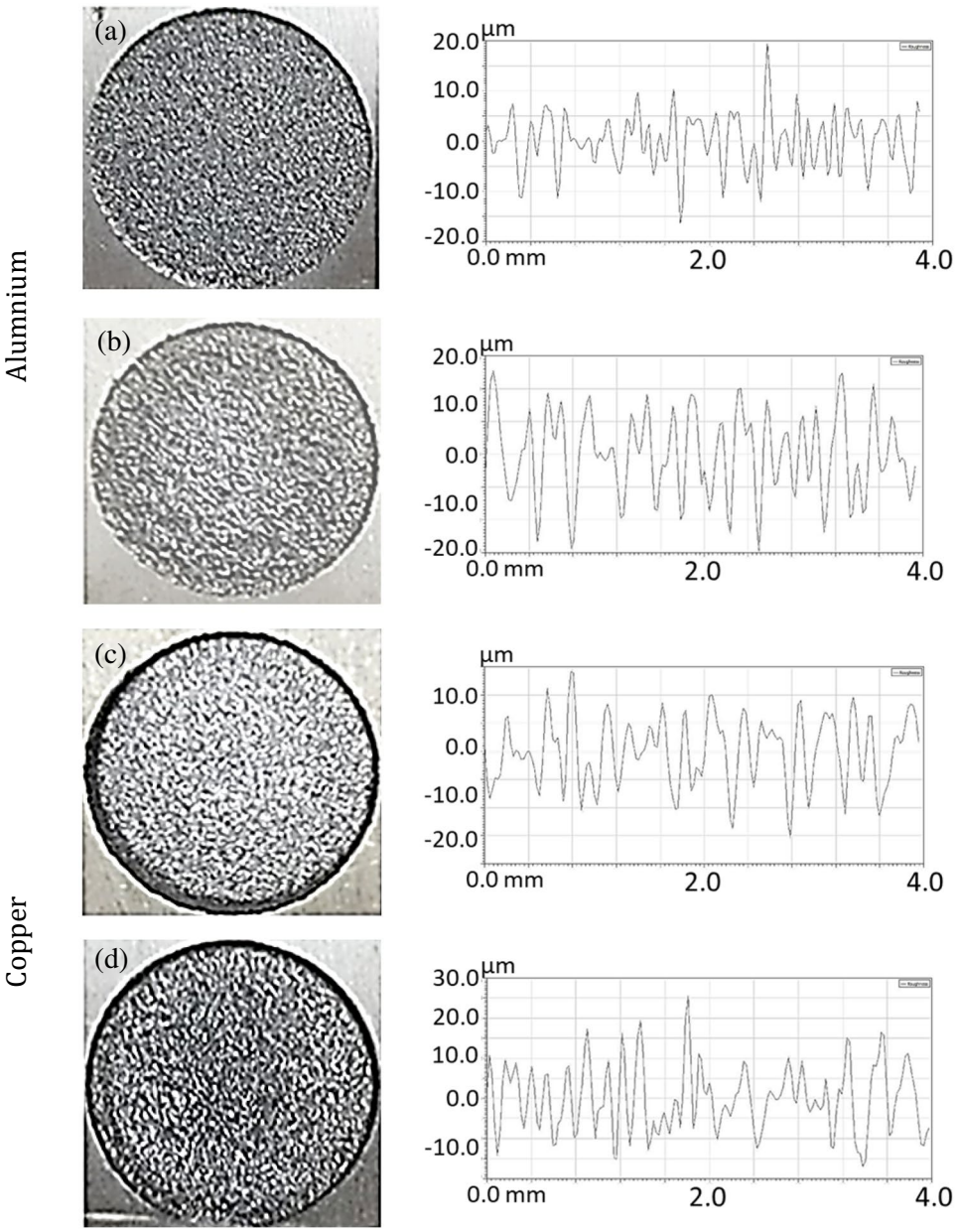

Fig. 3 Machined surfaces and profilograms at low and high Ra obtained with Al (a, b), Br (c, d), Cu (e, f), and Gr (g, h) electrodes

It can be inferred from Fig. 5 that aluminum has the lowest roughness Rt around 28 µm, as compared to all other electrodes, because of the lowest melting temperature of the electrode compared to the workpiece with a high melting temperature of 1660 °C. The highest roughness was generated by graphite electrode ~ 61 µm which can also be seen from morphological analysis presented in Fig. 6. Copper resulted less Rt roughness (~ 34 µm) ~ 22.22% compared to brass electrodes because of the high packing density and melting temperature of copper atoms than brass atoms.

Pulse current and pulse on time are related to discharge energy. Gupta et al. [34] investigated that the pulse current increase raises the discharge energy, increasing the debris accumulation on the workpiece. The increase will cause unstable sparking, which results in small and interconnected craters. A similar trend with respect to Ra is observed when increasing the pulse current from 10 to 14 A. The increase in pulse current decreased the peak-to-valley height by ~ 27.65%. However, the rise in the pulse on time from 50 to 125 µs increased the material erosion time with a higher intensity of plasma channel. This phenomenon resulted in an increase in Rt from 33 to 55 µm. Pulse off time followed a similar trend as Ra as it is linked with flushing characteristics. The adequate cleaning of the melt pool decreased 40% of the crater characteristics by resulting in Rt 33 µm at 100 µs. Positive polarity showed the more favorable condition of decreasing trend of Rt as compared to negative polarity as it is linked with the energy distribution principle [35].

Fig. 3 (continued)

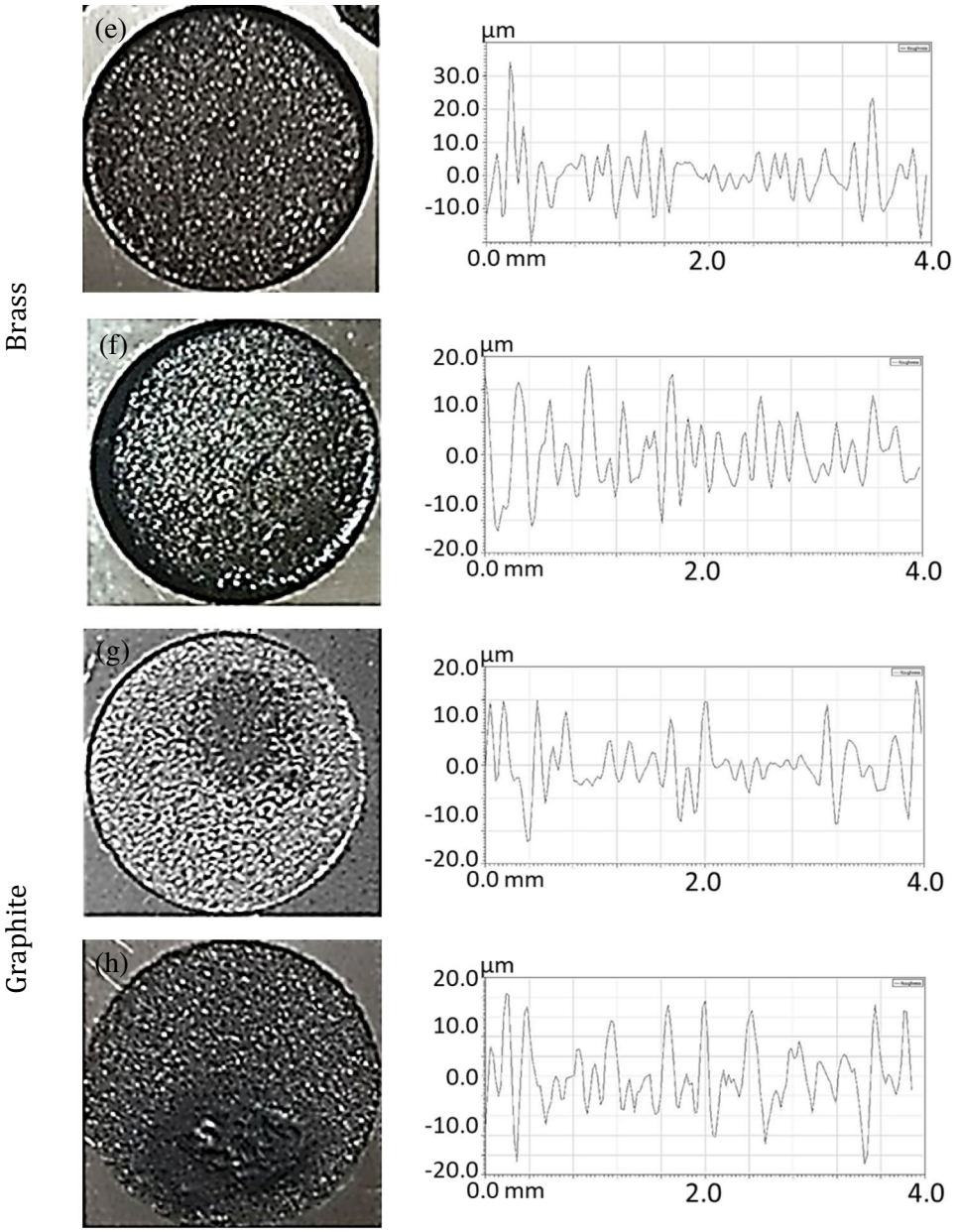

The process significantly depends on the thermos-physical attributes of workpiece and tool electrode. However, non-thermal attributes are not completely irrelevant depending upon mechanical effects and electric-dynamic properties. The surface machined through the graphite tool electrode is shown in Fig. 6. A high content of redeposits is evident which is of white color showing the formation of oxides during the flushing action. The graphite electrode produced high peak-to-valley distance because of its high melting temperature of 3300 °C as compared to Ti6Al4V 1660 °C. The synergistic effect of high thermal conductivity (400 W-m^{-1} K^{-1}) of graphite and low conductivity (6.7 W-m^{-1} K^{-1}) results in blockage of heat energy on the surface creating deeper and wider craters. Moreover, the breakdown of open circuit voltage between the powder particle and workpiece/tool results in sparking activity by emitting electrons from the cathode electrode. The electrons collide with kerosene molecules forming additional electrons and positive ions. The formation of high-energy plasma channel between the tool electrode-powder particle-workpiece results in the formation of metal oxides and carbides on the surface because of the reaction between melt and dielectric [36]. Therefore, considering the above mechanism, graphite is a stable cathode as compared to copper or other alternatives which promotes intense material removal resulting in deep and wider craters.

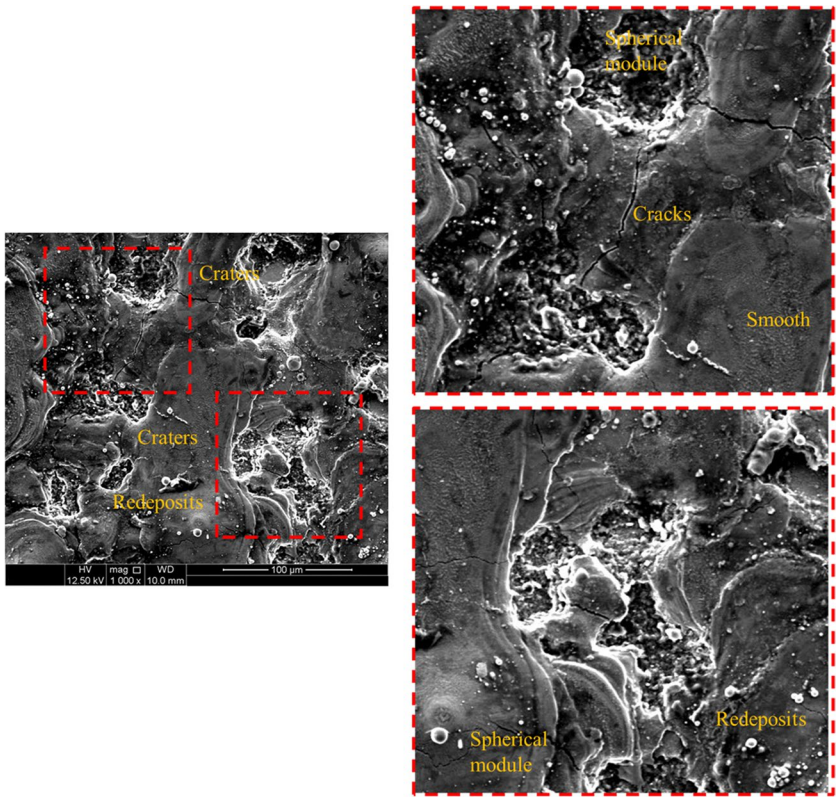

Fig. 4 Surface morphology produced by aluminum electrode, 14 A pulse current, 75 µs pulse on time, 75 µs pulse off time, and + ve polarity

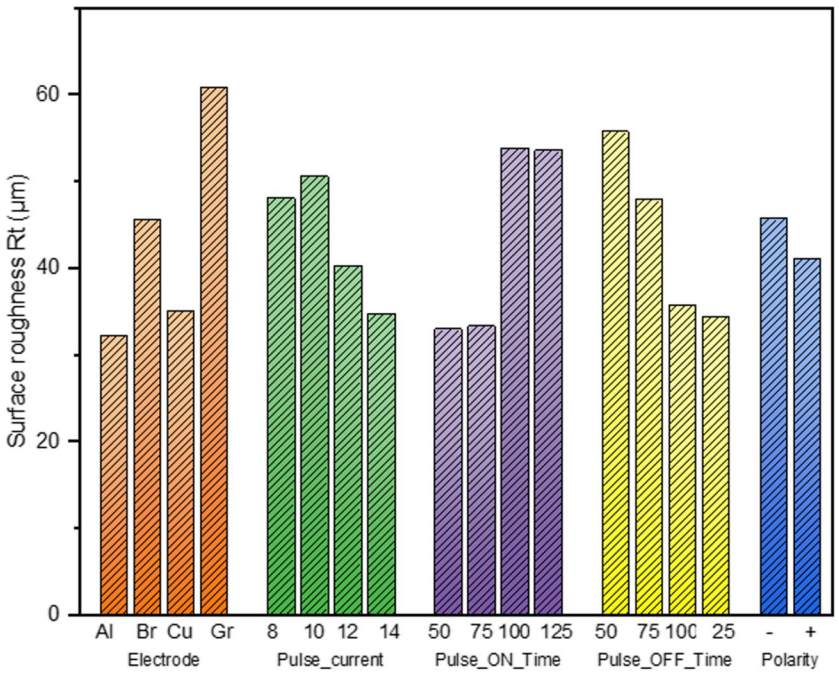

Fig. 5 Main effect plot for the highest peak and the deepest valley (Rt)

3.1.3 Roughness—average peak-to-valley distance Rz

The average peak-to-valley distance is analyzed to have a better understanding with respect to tribological needs. Since two surfaces slide on each other in tribological systems, the possibility of the wear increases if the surface has more peak heights. The overall trends are similar to Ra; however, the distances differ in several folds. Therefore, the peak-to-depth distance is important to characterize considering the variability of thermo-electrical properties of electrodes [37].

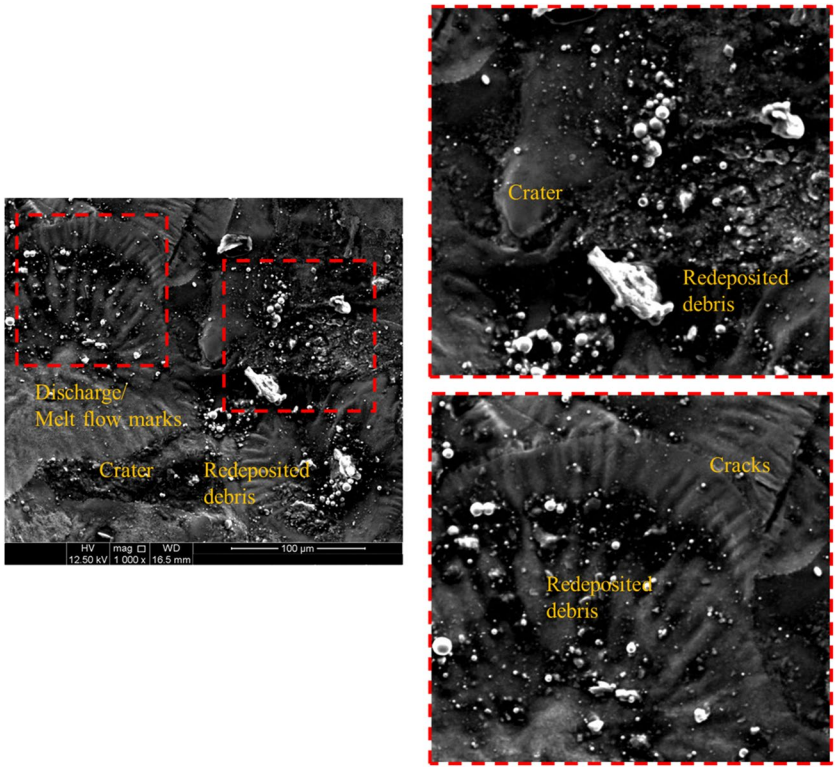

Fig. 6 Surface morphology produced by graphite electrode, 14 A pulse current, 75 µs pulse on time, 75 µs pulse off time, and + ve polarity

Electrode material and pulse on time are the 2nd and 3rd highest percentage contributors, which have been determined through analysis of variance (discussed in a later section) that affects the mean roughness depth. Graphite shows a 60% increase in Rz (44 µm) compared to aluminum. Graphite is thermally conductive with higher mobility of electrons. This results in the sparks going deeper into the surface and eroding the material. The intense spark with high discharge energy increased the peak-depth distance up to 42 µm about 90% when Po increased from 75 to 100 µs. The arcing and debris accumulation also influence the peaks and valley distribution [34]. Ramamurthy et al. [29] found that a higher pulse current produced deeper cavities with poor surface integrity. Likewise, Ahmed et al. [30] affirmed that balanced sparking with flushing action results in shallow craters with improved surface quality and lower roughness. Pulse off time controls Rz significantly and has the highest percentage contribution. The control indicates the need for improved flushing and adequate removal of the melt pool. With the increase in pulse off time from 25 to 75 µs, a relative decrease of 47% is observed. A similar descending trend is visible for the pulse current. The lowest Rz achieved at different conditions of the pulse off time is about 22 µm, as shown in Fig. 7. Therefore, to control the average roughness, peak-to-value distance, and surface integrity, a balanced distribution of discharge energy is needed. The aluminum electrode outperformed the surface characteristics in comparison to other electrodes. However, the surface attributes are strongly linked with cutting efficiency and erosion mechanism [9], requiring simultaneous optimization without compromising any objectives.

The machined surfaces produced through copper and brass are shown in Fig. 8 and Fig. 9, respectively. The surface obtained with copper electrode has a large degree of redeposits and carbon. The crack formation is less as compared to aluminum electrode. However, the redeposition of particles is significantly high as compared to other alternatives. The average peak-to-valley distance obtained by copper is comparable to aluminum and brass (derivative of copper with zinc). Whereas the brass produced wider craters with a high degree of cracks, the copper has a higher melting temperature of 1083 °C as compared to brass 940 °C and aluminum 660 °C. The craters are visible on the surface machined through brass because high tool degeneration results in higher roughness [7]. The tool is kept as the inverse of workpiece shape during electric discharge machining process which requires balanced thermal intensity and material removal of workpiece and tool. The copper electrode offers the highest electric conductivity 59.6×10^6 S-m^{-1} which ensures high conduction of electrons from the tool surface. The increased conductivity results in excessive sparking conditions which disintegrate dielectric fluid and increase melt volume. The mechanism results in the deposition of carbon on the surface. The other electrodes have not resulted comparable proportion of carbon on the surface, whereas the brass resulted in wide craters and cracking

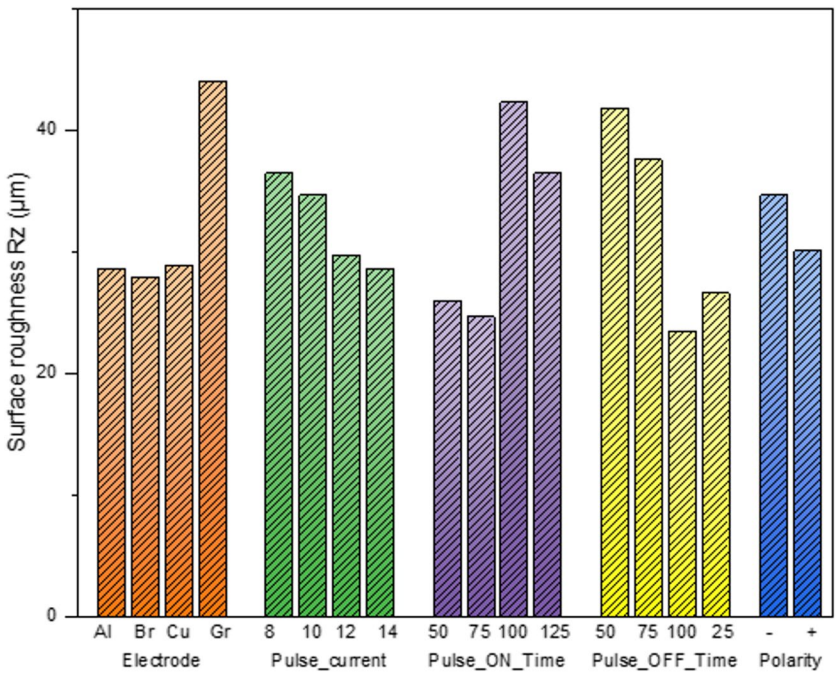

Fig. 7 Main effect plot for an average peak-to-valley distance (Rz (ISO))

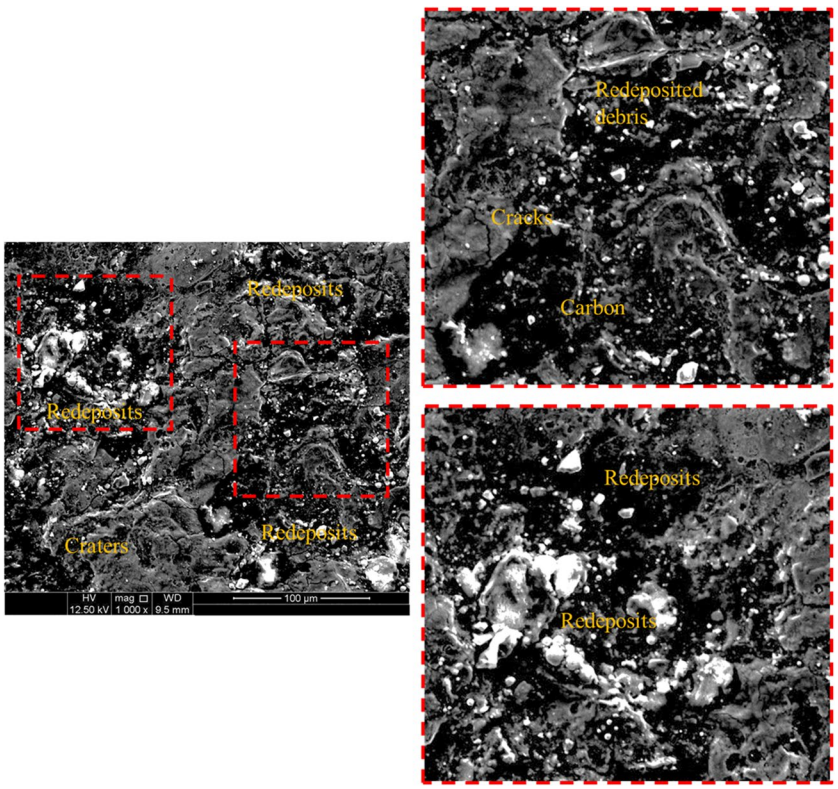

Fig. 8 Surface morphology produced by copper electrode, 14 A pulse current, 75 µs pulse on time, 75 µs pulse off time, and + ve polarity

resulting from poor thermal conductivity. The heat is confined in the interaction zone resulting in unbalanced melting of the workpiece surface.

Conclusively, the small and interconnected craters usually result from electro-thermal mechanism of discharge breakage. Similarly, the wider craters are the synergistic effect of poor thermal conduction of both tool and workpiece. The interconnected craters lower the roughness because of the support from thermal conductivity and low impulsive forces in the plasma channel. Therefore, branching of electric arcs, effective flushing attributes, and sufficient thermal conduction are required to machine the material with least surface defects.

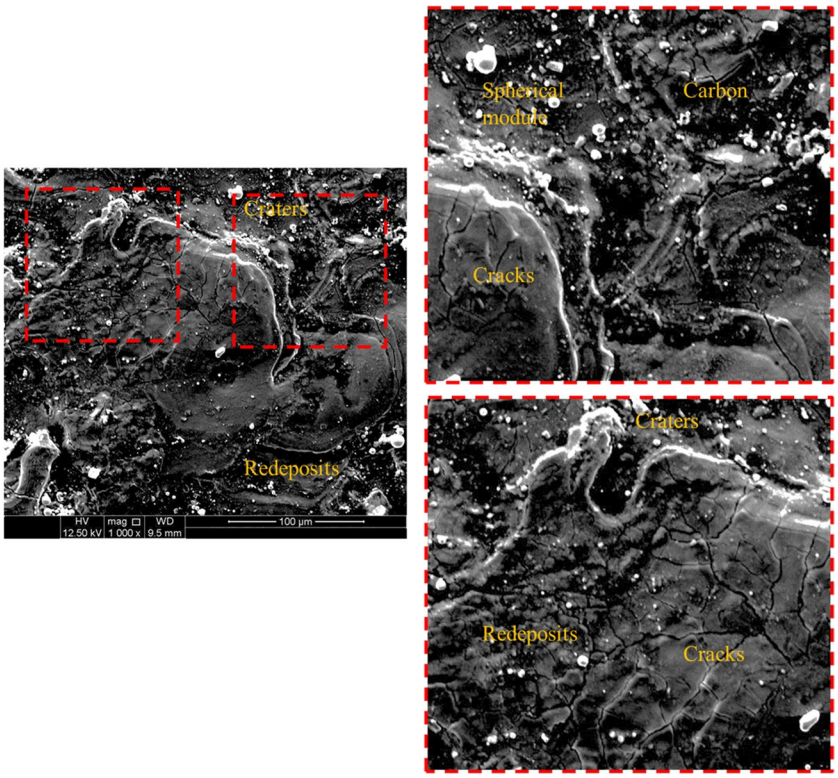

Fig. 9 Surface morphology produced by brass electrode, 14 A pulse current, 75 µs pulse on time, 75 µs pulse off time, and + ve polarity

3.1.4 Material removal rate

The highest material removal rate was obtained with the Br electrode, 12.20 mm^3/min, while Gr showed the second-highest, 3.06 mm^3/min. However, the Al electrode resulted in the least MRR among its competitors (Fig. 10). The reason behind this trend is the melting point difference between the workpiece and tool. The graphite electrode shows predictive behavior of the increase in heat dissipation rate in graphite electrodes compared to the workpiece. Heating in the interface of the small particle-sized sintered graphite results in improved surface generation with reduced porosity and

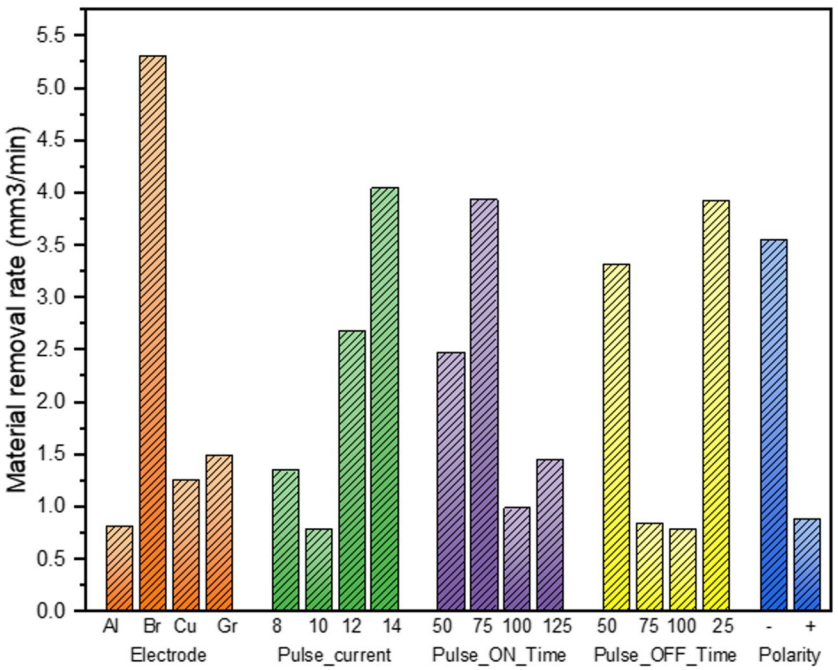

Fig. 10 Trend analysis of parametric levels for material removal rate

crack density. The interfacial energy erodes the surface with smaller and shallow craters, consequently lowering material removal by 2 mm^3/min compared to brass [38]. These tool materials show more damage in their geometry after the machining with more material removal rate, and rougher surfaces are generated as a result of machining [39].

Al electrode has a lower melting point (660 °C) than Ti6Al4V melting point (1660 °C), which promotes more material erosion and vaporization of tool material rather than workpiece material which reduces the material removal rate [40]. The choice of the brass electrode gives the highest MRR, about 5.5 mm^3/min. This increase is because of the different densities between the workpiece and tool electrode, as the density of brass is 8.73 g-cm^{-3} which is 65.33% greater than the density of Ti6Al4V. The bond strength of the workpiece electrode atoms is far smaller than brass electrode atoms which results in erosion of the workpiece surface compared to the tool electrode [7]. Although copper has more density as compared to brass, however, thermal conductivity of 385 W-m^{-1} K^{-1} of copper is more than brass and aluminum. The correlation between thermal conductivity and density helps brass to outperform. The dissipation heat reduces plasma intensity which affects workpiece erosion (Fig. 11). Therefore, the copper electrode resulted in ~ 1.2 mm^3/min owing to high thermal conductivity and high energy transmission rate through the atoms of electrode material. Graphite electrode has very unique electrical, thermal, and physical properties (Table 4) that is advantageous during machining as its melting point is 3300 °C as compared to the workpiece's 1660 °C. Dong et al. [41] concluded that the greater melting temperature difference increases the erosion of the workpiece. This results in reduced tool electrode wear. However, a lower density (1.77 g-cm^{-3}) graphite tool with a higher thermal conductivity of 400 W-m^{-1} K^{-1} hinders a higher material removal rate.

An increase in the pulse current showed the increasing linear trend for material removal since the upsurge generates the pool of intense discharge energy channel (Fig. 11). From the main effect plot, an increase in pulse current from 8 to 14 A provokes material vaporization. This phenomenon causes to increase in MRR from 1.2 to 4 mm^3/min. At high pulse current 12 A, the accumulation of debris because of the inefficient flushing process with less intense sparking resulted in a slight decrease in trend. The pulse on time 50 µs resulted in ~ 3 mm^3/min material removal rate. With the increase in pulse on time, energy transfer increased, which resulted increased 4 mm^3/min MRR (~ 33.33% increase). However, further increase in on time (75 to 100 µs) imbalanced the sparking and caused debris accumulation because of improper flushing action. This debris facilitates through widening the discharge energy column with a decrease in the discharge energy density at the material erosion drops down to 1.2 mm^3/min. This promoted the arcing effect and reduced the removal rate. Teimouri et al. [42] considered arcing phenomenon to reduce MRR at increased pulse on value.

At the lower pulse off time, 25 µs maximum erosion of the workpiece around 4 mm^3/min is observed in Fig. 10. An increase in the pulse off time resulted in the decreasing trend of material removal up to 0.75 mm^3/min due to compromised sparking to flushing ratio [30]. The negative polarity resulted in ~ 4 mm^3/min, which is significantly higher than the positive, where a 75% reduction was observed. The results are in line with the literature where negative polarity is recommended for higher MRR [41]. Cyril Pilligrin et al. [43] evaluated the effect of polarities on drilling the micro-holes in 316L steel where high MRR was observed with negative polarity. EDM typically involves the use of dielectric fluids to flush away eroded material and cool the workpiece. Some dielectric fluids may not be compatible with aluminum, leading to chemical reactions or contamination of the fluid, which can affect the overall process performance. But Al electrode can be used for specific application in EDM. Aluminum has a relatively high thermal conductivity compared to copper, brass, and graphite. This means that it can effectively dissipate the heat generated during the EDM process, preventing excessive localized heating of the workpiece [44, 44]. SiC powder added to the dielectric improves the machining efficiency by assisting in the melting and removal of recast layers from the workpiece surface. It acts as an abrasive material. Therefore, the combination of the high thermal conductivity of aluminum, the benefits of SiC powder in the dielectric, and the specific characteristics of titanium can create a synergistic effect that leads to an improved surface finish. On the other hand, aluminum has

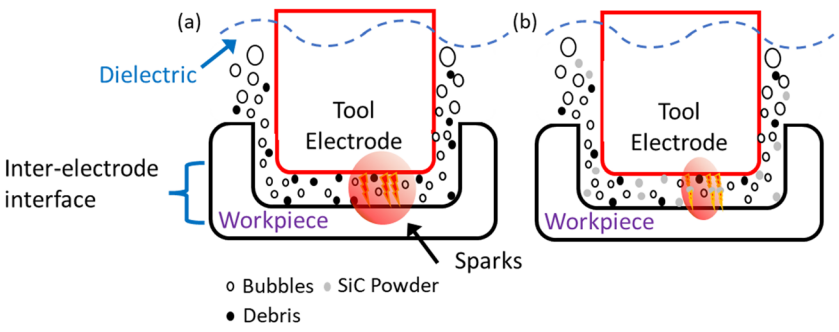

Fig. 11 Schematic of the electric spark erosion and surface wear phenomenon (**a**) without addition of powder and (**b**) with addition of powder

a lower melting point than titanium alloys like Ti6Al4V. Aluminum's relative erosion resistance compared to copper, brass, and graphite, combined with the effects of SiC powder, can lead to reduced electrode wear. There could be some intermixing or alloying between aluminum electrode and titanium workpiece at the microscopic level during repeated sparking. Aluminum reacts with oxygen in the dielectric and the EDM plasma to form aluminum oxide (Al_2O_3) [27, 45]. This oxide layer may form on the aluminum electrode surface, affecting its behavior and potentially introducing Al_2O_3 into the EDM. SiC powder can potentially decompose at high temperatures, releasing silicon (Si) and carbon (C) species. These released species could potentially react with other elements present in plasma, leading to the formation of compounds like silicon carbides or other Si-containing species [46, 47].

3.2 Parametric significance analysis

Analysis of variance (ANOVA) is carried out to estimate the relative impact of individual variables on all measured response parameters. *F*-value plays a significant role in showing the relative importance of input factors [30]. ANOVA tests the model's acceptability with a confidence level of 95% against the *P*-value, which should be less than 0.05 [31]. Apart from *P*-values, percentage contribution (PCR) is also determined, which illustrates the control of the specific response. The analysis of variance results for material removal rate depicts that electrode material, polarity, pulse current, and pulse off time are significant as their *P*-values are less than 0.05 at a confidence level of 95% (Table 7). The electrode material is the highest contributing factor having a PCR of 32.65%, followed by pulse off time, having a PCR of 21.92%. Furthermore, the analysis of the variance of surface roughness characteristics is carried out to understand the underlying phenomena which control the features of the surface. It is observed that electrode material, pulse current, pulse on time, and pulse off time are significant on the surface roughness parameter at a 95% confidence level. It reflects the significant contribution of controlling the morphology of the surface.

Firstly, the pulse on time (ON) is found to be the highest contributing factor (32.15%) to control arithmetic roughness, followed by pulse off time (28.40%). ANOVA results for Rt reveal that electrode material is the most contributing factor (38.87%), which controls the peaks and valley distance. The ANOVA results for Rz show that all parameters are significant, with pulse off time having the highest control, 32.82%, as flushing action contributes to form a recast layer and removal of the melt pool. Secondly, the pulse on time 30.93% and, thirdly, electrode material 26.66% influence significantly in controlling the surface features crucial for tribological requirements.

Table 7 ANOVA results for material removal rate and surface roughness parameters

Source	DF	*F*-value	*P*-value	PCR (%)	*F*-value	*P*-value	PCR (%)
Parameters		MRR			Ra		
El	3	51.05	0.019*	32.65%	70.61	0.014*	24.73%
PC	3	21.79	0.044*	13.94%	38.73	0.025*	13.57%
ON	3	14.93	0.063	9.55%	91.78	0.011*	32.15%
OFF	3	34.27	0.028*	21.92%	81.07	0.012*	28.40%
Po	1	100.93	0.010*	21.52%	7.83	0.108	0.91%
Error	2			0.43%			0.23%
Total	15			100.00%			100.00%
Model summary							
MRR	*R*-sq = 99.57%		*R*-sq(adj) = 96.80%				
Ra	*R*-sq = 99.77%		*R*-sq(adj) = 98.25%				
Parameters		Rt			Rz		
El	3	137.81	0.007*	38.87%	163.48	0.006*	26.66%
PC	3	33.74	0.029*	9.52%	40.49	0.024*	6.60%
ON	3	101.18	0.010*	28.54%	189.66	0.005*	30.93%
OFF	3	75.78	0.013*	21.37%	201.20	0.005*	32.82%
Po	1	16.08	0.057	1.51%	52.90	0.018*	2.88%
Error	2			0.19%			0.11%
Total	15			100.00%			100.00%
Model summary							
Rt	*R*-sq = 99.81%		*R*-sq(adj) = 98.59%				
Rz	*R*-sq = 99.89%		*R*-sq(adj) = 99.18%				

*Significant at 95% confidence level

3.3 Multi-response optimization

Considering the conflicting nature of the responses, multi-response optimization is needed to better optimize problems with multiple responses and process parameters. Therefore, the grey relational analysis is one of the multi-objective approaches which has been applied to different fields because of its capability to result in balanced compromise. The grey relational analysis starts by normalizing experimental results (surface roughness and MRR) in the range of zero to one, a process known as a grey relational generation. The grey relational coefficient is computed from the normalized experimental data to describe the link between the desired and actual experimental data. The grey relational grade (GRG) is then calculated by averaging each process response's grey relational coefficient. The grey relational grade assesses the overall quality of the many process outcomes. Consequently, the optimization of several complex process responses may be reduced to the optimization of a single grey relational grade. In this technique, the linear data preprocessing method for MRR, which is higher-the-better, was expressed as Eq. 1.

$$x_i(m) = \frac{y_i(m) - \min y_i(m)}{\max y_i(m) - \min y_i(m)} \tag{1}$$

Similarly, surface roughness is lower-the-better and can be expressed as Eq. 2:

$$x_i(m) = \frac{\max y_i(m) - y_i(m)}{\max y_i(m) - \min y_i(m)} \tag{2}$$

where $x_i(m)$ is the value after the grey relation generation, $\min y_i(m)$ is the smallest value of $y_i(m)$ for the mth response, and $\max y_i(m)$ is the largest value of $y_i(m)$ for the mth response. An ideal sequence is $x_0(m)$(m = 1, 2, …9) for surface roughness and MRR. The definition of grey relation generation is to show the relational degree between the nine sequences [$x_0(m)$ and $x_i(m)$, i = 1, 2, …9: m = 1, 2, …9]. The grey relational coefficient $\xi_i(m)$ can be calculated as Eq. 3:

$$\xi_i(m) = \frac{\Delta_{\min} + \zeta \Delta_{\max}}{\Delta_{0i}(m) + \zeta \Delta_{\max}} \tag{3}$$

where Δ_{0i}=‖‖$x_0(m)$-$x_i(m)$‖‖ is the difference of the absolute value between $x_0(m)$ and $x_i(m)$; ζ is the distinguishing coefficient (0 ~ 1); $\Delta_{\min}$ is the small value of Δ_{0i}; and $\Delta_{\max}$ is the largest value of Δ_{0i} [22]. After averaging the grey relational coefficients, the grey relational grade γ_i can be obtained as Eq. 4:

$$\gamma_i = \frac{1}{n} \sum_{k=1}^{n} \varepsilon_i(m) \tag{4}$$

Here, the ranking is calculated based on the highest values of GRG. The level with the highest rank shows optimum parametric levels. Normalizing sequence, deviation sequence, grey relational coefficients (GRCs), GRD, and ranking for all experimental conditions are listed in Table 8.

It can be seen from the data (Table 8) that experiment number 5 conditions obtained the highest rank. These conditions are Cu electrode, 8 A pulse current, 75 µs pulse on time, 75 µs pulse off time, and negative polarity. From the ANOVA results of GRA (Table 9), it can be seen that all factors are statistically significant, with a pulse on time being the most significant parameter having a PCR of 46.76%. Similarly, the pulse off time and electrode materials controlled 19.88% and 19.76% of all responses, respectively. The polarity was found the least contributing factors

Table 8 Grey relational analysis results

Exp. no	Normalizing				Deviation sequence				Grey relational coefficient				GRG	Rank
	MRR	Ra	Rt	Rz	MRR	Ra	Rt	Rz	MRR	Ra	Rt	Rz		
1	0.00	0.72	0.84	0.67	1.00	0.28	0.16	0.33	0.33	0.64	0.76	0.60	0.586	11
2	0.04	0.89	1.00	0.90	0.96	0.11	0.00	0.10	0.34	0.81	0.99	0.84	0.746	5
3	0.02	0.91	0.92	0.80	0.98	0.09	0.08	0.20	0.34	0.85	0.86	0.71	0.690	9
4	0.09	0.97	0.99	0.88	0.91	0.03	0.01	0.12	0.36	0.95	0.98	0.81	0.774	4
5	0.07	1.02	1.01	1.00	0.93	0.02	0.01	0.00	0.35	1.03	1.01	1.00	0.849	1
6	0.02	1.00	0.98	0.93	0.98	0.00	0.02	0.07	0.34	1.00	0.97	0.88	0.797	3
7	0.07	0.68	0.56	0.61	0.93	0.32	0.44	0.39	0.35	0.61	0.53	0.56	0.514	13
8	0.09	0.66	0.82	0.64	0.91	0.34	0.18	0.36	0.36	0.60	0.74	0.58	0.568	12
9	0.00	0.62	0.60	0.66	1.00	0.38	0.40	0.34	0.33	0.57	0.56	0.59	0.513	14
10	0.00	0.89	0.62	0.93	1.00	0.11	0.38	0.07	0.33	0.82	0.57	0.88	0.651	10
11	0.72	0.91	0.79	0.81	0.28	0.09	0.21	0.19	0.64	0.84	0.70	0.73	0.730	6
12	1.00	0.92	0.75	0.82	0.00	0.08	0.25	0.18	1.00	0.86	0.67	0.74	0.817	2
13	0.22	0.20	0.16	0.20	0.78	0.80	0.84	0.80	0.39	0.38	0.37	0.39	0.383	15
14	0.18	0.03	0.00	0.00	0.82	0.97	1.00	1.00	0.38	0.34	0.33	0.33	0.346	16
15	0.05	0.96	0.86	0.88	0.95	0.04	0.14	0.12	0.34	0.93	0.78	0.81	0.718	7
16	0.03	0.94	0.85	0.88	0.97	0.06	0.15	0.12	0.34	0.90	0.77	0.80	0.703	8

Table 9 ANOVA table for GRG

Source	DF	*F*-value	*P*-value	PCR (%)
El	3	154.92	0.006*	19.76%
PC	3	84.27	0.012*	10.75%
ON	3	366.57	0.003*	46.76%
OFF	3	155.84	0.006*	19.88%
Po	1	64.76	0.015*	2.75%
Error	2			0.09%
Total	15			100.00%

*Significant (*R*-sq = 99.91%, *R*-sq(adj) = 99.36%)

as compared to others. The *R*-sq value 99.91% and *R*-sq(adj) 99.36% show the model's adequacy which highlights that all data points are predictable with minimal error percentage.

The response results of means for GRG (Fig. 12) represent that pulse on time at level 2 affects more than other parameters. The main effect plot (Fig. 12) reveals the highest GRG mean achieved with the Al electrode, pulse current of 14 A, pulse on time of 75 µs, pulse off time of 75 µs, and negative polarity condition. The confirmatory experiments on the settings recommended by the grey relational grade have been carried out to second the analysis.

4 Conclusions

The study has been carried out to investigate the potentiality of electric discharge machining of Ti6Al4V for tribological applications. A wide range of process parameters, including four types of electrodes, have been evaluated to quantify the influence over different surface parameters. Based on thorough experimental results, the following conclusions are drawn:

1. The increase in pulse on time at 100 µs erodes more material with deeper craters, and Ra rose to ~ 8.7 µm. At 75 µs and 125 µs decreasing trend in Ra, values were observed due to debris accumulation between the inter-electrode gap.
2. The aluminum has resulted the lowest roughness Rt around 28 µm because of the lowest melting temperature of the electrode compared to the workpiece with a high melting temperature of 1660 °C. Copper resulted less Rt roughness (~ 34 µm) ~ 22.22% compared to brass electrodes because of their different compositions and structures. Brass contains two different types of atoms (copper and zinc) that can create irregularities in its crystal lattice, contributing to its slightly rougher texture compared to pure copper. Copper, being a single-element metal, has a more uniform and regular atomic arrangement, leading to a smoother surface. Brass has a lower melting point than pure copper due to the presence of zinc, which can make its surface slightly softer and more prone to deformation, potentially contributing to a slightly rougher feel.
3. In essence, the composition and crystal structure of the materials are the primary factors causing the difference in roughness between copper and brass, rather than packing density or melting point.

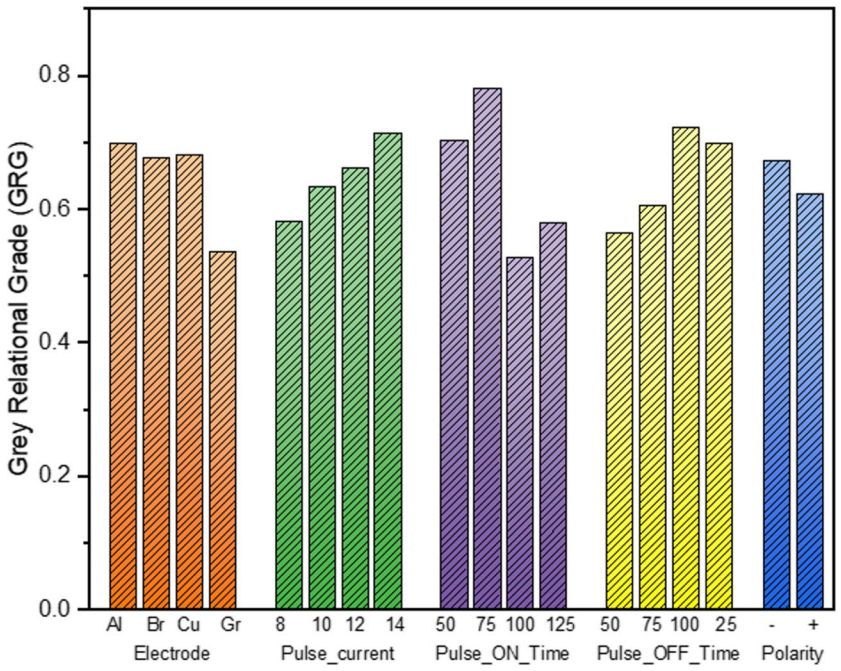

Fig. 12 Main effect plot for grey relational grade

4. The analysis of the variance of material removal rate depicts that electrode material, polarity, pulse current, and pulse off time are significant at a confidence level of 95%. The electrode material is the highest contributing factor having a PCR of 32.65%, followed by pulse off time, having a PCR of 21.92%. Similarly, the pulse on time is the highest contributing factor (32.15%) to control arithmetic roughness, followed by pulse off time (28.40%).
5. The machined surface with brass electrode possessed higher craters and cracks than the copper electrode. Likewise, a higher surface roughness was observed on the surface machined with Br than copper in terms of Ra and Rt, 5.45% and 36.36%, respectively.
6. Through grey relational analysis-based multi-response optimization, an optimal compromise between surface attributes and cutting efficiency is identified by Al electrode, pulse current of 14 A, pulse on time of 75 µs, pulse off time of 75 µs, and negative polarity parametric conditions.

The research could be extended by taking into account the possibility of plasma chemical reactions that significantly affect the condition of the treated surface, especially when using an assisting powder.

Author contribution Conceptualization, M.U.F. and M.A.A.; methodology, M.U.F. and S.A.; data curation, M.A.A., A.H., and R.T.M.; software, A.H. and R.T.M.; formal analysis, M.U.F. and S.A.; writing—original draft preparation, M.U.F.; writing—review and editing, M.U.F., M.A.A., and S.A. All authors read and approved the final manuscript.

Acknowledgements The authors appreciate the support from Researchers Supporting Project number (RSPD2023R702), King Saud University, Riyadh, Saudi Arabia.

Data availability The data is already available.

Code availability Not applicable.

Declarations

Ethics approval Not applicable.

Consent for publication All authors agreed upon the current version of the submission for publication.

Conflict of interest The authors declare no competing interests.

References

1. Farooq MU, Anwar S, Hurairah A (2023) Reducing micro-machining errors during electric discharge machining of titanium alloy using nonionic liquids. Mater Manuf Processes 0:1–16. https://doi.org/10.1080/10426914.2023.2236199
2. Farooq MU, Anwar S, Ullah R, Guerra RH (2023) Sustainable machining of additive manufactured SS-316L underpinning low carbon manufacturing goal. J Market Res 24:2299–2318. https://doi.org/10.1016/j.jmrt.2023.03.122
3. Javid H, Jahanzaib M, Jawad M et al (2021) Parametric analysis of turning HSLA steel under minimum quantity lubrication (MQL) and nanofluids-based minimum quantity lubrication (NF-MQL): a concept of one-step sustainable machining. Int J Adv Manuf Technol 117:1915–1934
4. Li L, Zhao L, Li ZY et al (2017) Surface characteristics of Ti-6Al-4V by SiC abrasive-mixed EDM with magnetic stirring. Mater Manuf Processes 32:83–86. https://doi.org/10.1080/10426914.2016.1151043
5. Bui VD, Mwangi JW, Schubert A (2019) Powder mixed electrical discharge machining for antibacterial coating on titanium implant surfaces. J Manuf Process 44:261–270. https://doi.org/10.1016/j.jmapro.2019.05.032
6. Mughal MP, Farooq MU, Mumtaz J et al (2021) Surface modification for osseointegration of Ti6Al4V ELI using powder mixed sinking EDM. J Mech Behav Biomed Mater 113:104145
7. Ahmed N, Anwar S, Ishfaq K et al (2019) The potentiality of sinking EDM for micro-impressions on Ti-6Al-4V: keeping the geometrical errors (axial and radial) and other machining measures (tool erosion and work roughness) at minimum. Sci Rep 9:1–19. https://doi.org/10.1038/s41598-019-52855-6
8. Al-Amin M, Abdul-Rani AM, Danish M et al (2021) Analysis of hybrid HA/CNT suspended-EDM process and multiple-objectives optimization to improve machining responses of 316L steel. J Market Res 15:2557–2574. https://doi.org/10.1016/j.jmrt.2021.09.074
9. Goyal KK, Sharma N, Gupta RD et al (2022) Measurement of performance characteristics of WEDM while processing AZ31 Mg-alloy using Levy flight MOGWO for orthopedic application. Int J Adv Manuf Technol. https://doi.org/10.1007/s00170-021-08358-8
10. Baroi BK, Jagadish, Patowari PK (2023) Effect of boric acid in powder mixed EDM of Ti-6al-4V ELI. Mater Manuf Processes 0:1–14. https://doi.org/10.1080/10426914.2023.2195907
11. Işık AT, Çakıroğlu R, Günay M (2023) Multiresponse optimization of performance indicators through Taguchi-grey relational analysis in EDM of cemented carbide. CIRP J Manuf Sci Technol 41:490–500. https://doi.org/10.1016/j.cirpj.2023.01.012
12. Bhowmick S, Mondal R, Sarkar S et al (2023) Parametric optimization and prediction of MRR and surface roughness of titanium mixed EDM for Inconel 718 using RSM and fuzzy logic. CIRP J Manuf Sci Technol 40:10–28. https://doi.org/10.1016/j.cirpj.2022.11.002
13. Guu YH, Hocheng H, Chou CY, Deng CS (2003) Effect of electrical discharge machining on surface characteristics and machining damage of AISI D2 tool steel. Mater Sci Eng, A 358:37–43
14. Gattu SD, Yan J (2022) Micro electrical discharge machining of ultrafine particle type tungsten carbide using dielectrics mixed

with various powders. Micromachines 13:998. https://doi.org/10.3390/mi13070998
15. Pradhan BB, Masanta M, Sarkar BR, Bhattacharyya B (2009) Investigation of electro-discharge micro-machining of titanium super alloy. Int J Adv Manuf Technol 41:1094–1106
16. Ekmekci N, Efe Y (2022) The effect of nano and micro hydroxyapatite powder additives on surface integrity in electrical discharge machining of Ti6Al4V alloy. Surf Coat Technol 445:128708. https://doi.org/10.1016/j.surfcoat.2022.128708
17. Surya MS, Gugulothu SK (2023) Investigations on powder mixed electrical discharge machining of aluminum alloy 7075–4 wt. % TiC in-situ metal matrix composite. Int J Interact Des Manuf 17:299–305. https://doi.org/10.1007/s12008-022-00895-0
18. Kumar PA, Vivek J, Senniangiri N et al (2022) A study of added SiC powder in kerosene for the blind square hole machining of CFRP using electrical discharge machining. SILICON 14:1831–1849. https://doi.org/10.1007/s12633-021-01243-9
19. urRehman A, Arif W, Hussain MI et al (2022) Analysis of particle size and concentration in die sinking electric discharge machining. Materials 15:4932. https://doi.org/10.3390/ma15144932
20. Darji RS, Joshi GR, Hembrom S et al (2022) Powder mixed electrical discharge machining of Inconel 718: investigation on material removal rate and surface roughness. Int J Interact Des Manuf. https://doi.org/10.1007/s12008-022-01059-w
21. Vora J, Khanna S, Chaudhari R et al (2022) Machining parameter optimization and experimental investigations of nano-graphene mixed electrical discharge machining of nitinol shape memory alloy. J Market Res 19:653–668. https://doi.org/10.1016/j.jmrt.2022.05.076
22. Majumdar S, Bhoi NK, Singh H (2022) Graphene nano-powder mixed electric discharge machining of Inconel 625 alloy: optimization of process parameters for material removal rate. Int J Interact Des Manuf. https://doi.org/10.1007/s12008-022-00996-w
23. Thakur SS, Pradhan SK, Sehgal S, Saxena KK (2023) Experimental investigations on silicon carbide mixed electric discharge machining. SILICON 15:583–601. https://doi.org/10.1007/s12633-022-02022-w
24. Kumar S, Goud M, Suri NM (2022) Grey relational analysis-based multi-response optimization of magnetic-field-assisted powder-mixed electric discharge machining of Inconel 706. Arab J Sci Eng 47:8315–8339. https://doi.org/10.1007/s13369-021-06204-3
25. Chakraborty S, Mitra S, Bose D (2022) Performance characterization of powder mixed wire electrical discharge machining technique for processing of Ti6Al4V alloy. Proc Inst Mech Eng, Part E: J Process Mech Eng 236:1283–1295. https://doi.org/10.1177/09544089211060722
26. Ishfaq K, Farooq MU, Pruncu CI (2021) Reducing the geometrical machining errors incurred during die repair and maintenance through electric discharge machining (EDM). Int J Adv Manuf Technol 117:3153–3168
27. Farooq MU, Bhatti HA, Asad M et al (2022) Surface generation on titanium alloy through powder-mixed electric discharge machining with the focus on bioimplant applications. Int J Adv Manuf Technol 122:1395–1411. https://doi.org/10.1007/s00170-022-09927-1
28. Farooq MU, Anwar S, Bhatti HA et al (2023) Electric discharge machining of Ti6Al4V ELI in biomedical industry: parametric analysis of surface functionalization and tribological characterization. Materials 16:4458
29. Ramamurthy A, Sivaramakrishnan R, Muthuramalingam T, Venugopal S (2015) Performance analysis of wire electrodes on machining Ti-6Al-4V alloy using electrical discharge machining process. Mach Sci Technol 19:577–592
30. Ahmed N, Ishfaq K, Moiduddin K et al (2019) Machinability of titanium alloy through electric discharge machining. Mater Manuf Processes 34:93–102. https://doi.org/10.1080/10426914.2018.1532092
31. Dong H, Li M, Liu T et al (2019) Mechanism study of sinking electrical discharge machining using water-in-oil nanoemulsion. Int J Adv Manuf Technol 105:2309–2320. https://doi.org/10.1007/s00170-019-04468-6
32. Ehsan S, Rehman M, Mughal MP et al (2023) Correction: Machinability investigations through novel controlled flushing characteristics in wire electric discharge machining of M42 high-speed steel. Int J Adv Manuf Technol 128:4717–4719. https://doi.org/10.1007/s00170-023-12294-0
33. Salcedo AT, Arbizu IP, Luis Pérez CJ (2017) Analytical modelling of energy density and optimization of the EDM machining parameters of inconel 600. Metals 7:. https://doi.org/10.3390/met7050166
34. Gupta P, Gupta R, Khanna R, Sharma N (2012) Effect of process parameters on Kerf width in WEDM for HSLA using response surface methodology. J Eng Technol 2:1. https://doi.org/10.4103/0976-8580.94230
35. Singh S, Maheshwari S, Pandey PC (2004) Some investigations into the electric discharge machining of hardened tool steel using different electrode materials. J Mater Process Technol 149:272–277. https://doi.org/10.1016/j.jmatprotec.2003.11.046
36. Philip JT, Mathew J, Kuriachen B (2021) Transition from EDM to PMEDM – impact of suspended particulates in the dielectric on Ti6Al4V and other distinct material surfaces: a review. J Manuf Process 64:1105–1142. https://doi.org/10.1016/j.jmapro.2021.01.056
37. Mitutoyo (2010) Quick guide to surface roughness measurement: reference guide for laboratory and workshop. Mitutoyo America Corporation 1:1–8
38. Bhaumik M, Maity K (2018) Effect of different tool materials during EDM performance of titanium grade 6 alloy. Eng Sci Technol, an Int J 21:507–516. https://doi.org/10.1016/j.jestch.2018.04.018
39. Samuel MP, Philip PK (1997) Power metallurgy tool electrodes for electrical discharge machining. Int J Mach Tools Manuf 37:1625–1633
40. Vaseekaran S, Brown CA (1996) Single discharge, spark erosion in TiB2 and zinc part I: experimental. J Mater Process Technol 58:70–78
41. Dong H, Liu Y, Li M et al (2019) Sustainable electrical discharge machining using water in oil nanoemulsion. J Manuf Process 46:118–128. https://doi.org/10.1016/j.jmapro.2019.08.035
42. Teimouri R, Baseri H (2012) Study of tool wear and overcut in EDM process with rotary tool and magnetic field. Adv Tribol 895918. https://doi.org/10.1155/2012/895918
43. Cyril Pilligrin J, Asokan P, Jerald J et al (2017) Tool speed and polarity effects in micro-EDM drilling of 316L stainless steel. Prod Manuf Res 5:99–117
44. Farooq MU, Anwar S, Kumar MS et al (2022) A novel flushing mechanism to minimize roughness and dimensional errors during wire electric discharge machining of complex profiles on Inconel 718. Materials 15:7330. https://doi.org/10.3390/ma15207330
45. Asif N, Saleem MQ, Farooq MU (2023) Performance evaluation of surfactant mixed dielectric and process optimization for electrical discharge machining of titanium alloy Ti6Al4V. CIRP J Manuf Sci Technol 43:42–56. https://doi.org/10.1016/j.cirpj.2023.02.007
46. Farooq MU, Anwar S (2023) Investigations on the surface integrity of Ti6Al4V under modified dielectric(s)-based electric discharge machining using cryogenically treated electrodes. Processes 11:877. https://doi.org/10.3390/pr11030877
47. Umar Farooq M, Pervez Mughal M, Ahmed N et al (2020) On the investigation of surface integrity of Ti6Al4V ELI using Si-mixed electric discharge machining. Materials 13:1549. https://doi.org/10.3390/ma13071549